JOURNAL OF MATERIALS SCIENCE 32 (1997) 3841–3850

Residual stress and thermal properties of zirconia/metal (nickel, stainless steel 304) functionally graded materials fabricated by hot pressing

YEON-GIL JUNG, SUNG-CHURL CHOI, CHANG-SEOB OH
Department of Inorganic Materials Engineering, Hanyang University, Seoul 133-791, Korea

UN-GYU PAIK
Ceramics Division, Materials Building 223, NIST, Gaithersburg, MD 20899, USA

To analyse the residual stress and the thermal properties of functionally graded materials (FGMs), disc-type tetragonal zirconia polycrystal (TZP)/Ni- and TZP/stainless steel 304 (SUS304)-FGM were hot pressed, and compared with directly jointed materials (DJMs). The continuous interface and the microstructure of FGMs were characterized by electron probe microanalysis, wavelength dispersive spectrometry, optical microscopy and scanning electron microscopy. It has been verified that the defect-like cracks in FGMs are induced by the preferential shear stress and shown to cause fracture. These facts have corresponded well with the residual stress distribution analysed by the finite element method. The thermal diffusivity and the thermal conductivity of FGMs and DJMs were also measured by the laser flash technique. As a consequence, this work has described the interfacial stability, the residual stress release mechanism and the thermal protection characteristics of FGMs via a compositional gradient.

1. Introduction

A wide temperature deviation between the inner and outer surfaces is built up in materials which are applied under aerospace environments. For this reason, a severe residual stress is induced in these materials. The major requirements in the designing of materials used under the above-mentioned environments are heat resistance, high-temperature strength, thermal shock resistance and anti-corrosion, etc. [1–5]. As one of these materials, ceramic/metal composite has come to the fore [2, 3]. On the other hand, conventional thermal barrier coating and direct ceramic/metal joining are usually unsuccessful because of the fracture and/or the spallation of the ceramic layer due to an excessive residual stress generated near the interface. In particular, if the tensile stress is formed at the interface or ceramic region, it is fatal to the material itself [2, 6–12]. Therefore, in an effort to resolve these problems, the development of functionally gradient materials (FGMs) having a compositional graded from one surface of the material to the other, has been motivated [13–19]. In FGMs, the composition of a dispersion phase is gradually varied as a consequence, and thus the properties/microstructure relationship has a continuous characteristic. These features of FGMs are expected to reduce and/or eliminate the residual stress, as well as to control thermal barrier characteristics.

In this work, we chose the 3 mol % Y_2O_3-doped ZrO_2 (TZP) as the candidate ceramic material, which has excellent thermal barrier properties, anti-corrosion and wear resistance. As shown in Fig. 1, two sorts of metal were selected to examine the residual stress due to the thermal expansion mismatch between TZP and metal. The selected metals generate compressive stress at the interface or within the ceramic body in the direct joining of TZP/metal [20]. One is nickel, which may provide the relatively large critical defect size because of a similar coefficient of thermal expansion (CTEs) to that of TZP. The other is stainless steel 304 (SUS304). This may provide a smaller critical defect size than nickel, but has more varied applications. The effects of residual stress on the fracture of FGMs were investigated extensively to understand the various problems in terms of the fabrication process and the application of FGMs. The stress distribution of FGMs induced on cooling from the sintering temperature was analysed by the finite element method (FEM), and compared with directly jointed materials (DJMs). The thermal properties of FGMs and DJMs obtained by the laser flash technique were also measured to examine their potential as thermal barrier materials.

0022–2461

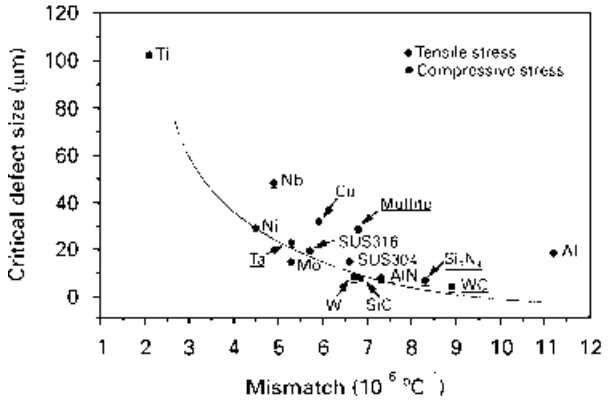

Figure 1 Effect of the coefficient of thermal expansion mismatch on critical defect size in TZP-metal and TZP-ceramic joining at 1250 °C [20].

2. Experimental procedure

The starting materials were 3 mol % Y_2O_3-doped tetragonal zirconia polycrystal (TZP: TZ-3Y, Tosoh Corp., Japan), nickel (Nilaco Corp., Japan) and SUS304 (Nilaco Corp., Japan) powders. The properties of the starting materials are shown in Table I. As a cost-efficient technology which is well known in industry and needs no extraordinary special equipment, the powder metallurgy (P/M) method was utilized [4, 21–24]. TZP and metals (nickel or SUS304) were mixed in isopropyl alcohol with 10 vol % compositional gradient, and then ball-milled for 12 h with 3Y-TZP milling media. After ball-milling, controlled particles of TZP (0.13 μm), nickel (5.65 μm) and SUS304 (5.11 μm) could be obtained, as shown in Fig. 2. To prevent inhomogeneous dispersion occurring due to the difference in density between two powders during the drying, the slurry was dried in a water-bath using a bar stirrer up to full viscosity without segregation. The green bodies of each composition were fabricated at an optimized pressure ($\leqslant 0.5$ ton mm^{-2}) using a disc-type steel die. When the composition of the metal was above 90 vol %, 1 wt % polyvinyl alcohol (PVA) was added for forming green bodies. The prepared disc-type green bodies of each composition were stacked in a graphite sleeve with

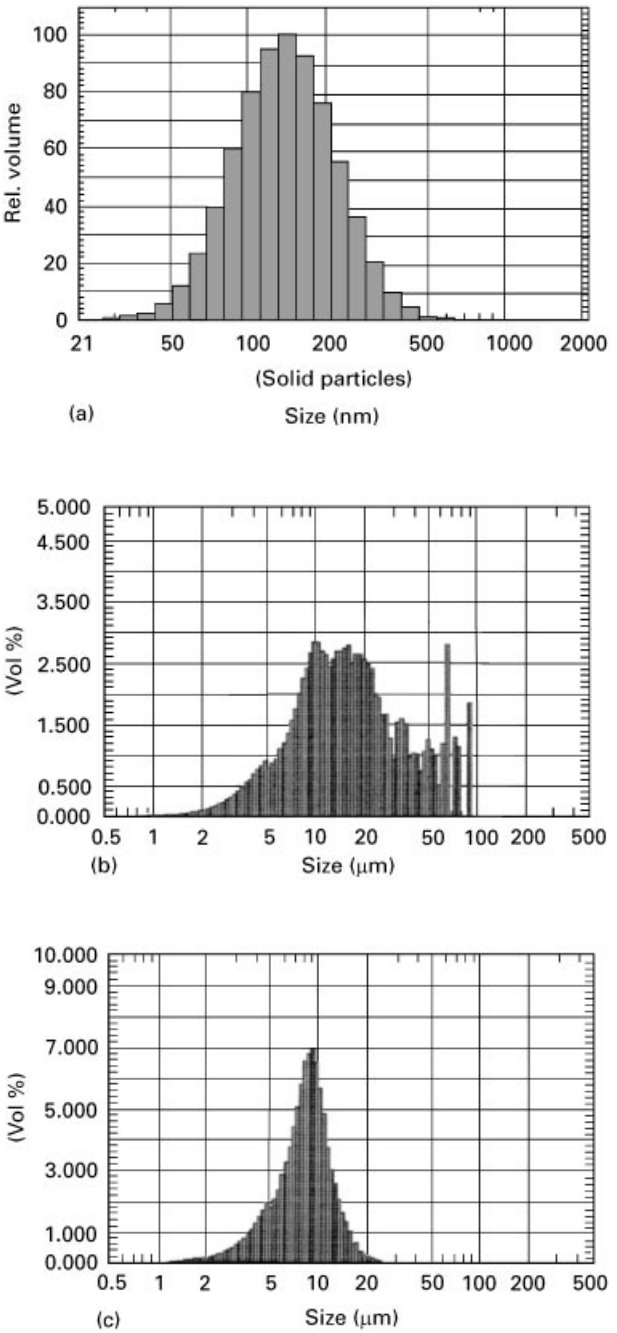

Figure 2 Particle size distribution of starting materials: (a) TZP, mean particle size = 0.13 μm; (b) Ni, mean particle size = 5.65 μm; (c) SUS304, mean particle size = 5.11 μm.

TABLE I Properties of raw materials

Materials	Density (10^3 kg m^{-3})	Melting point (°C)	Thermal conductivity (W m^{-1} K^{-1})	Average coefficient of thermal expansions (10^{-6} °C^{-1})	Modulus of elasticity (GPa)	Poisson's ratio	Mean particle size (μm)
TZP[a]	6.05	2715	3.3 (20 °C) 2.9 (600 °C) 2.3 (1000 °C)	9.6 (20–400 °C) 11.8 (20–1000 °C)	186 (20 °C)	0.31	0.3
SUS304[b]	8.06	1400–1450	16.2 (20–100 °C) 21.5 (20–500 °C)	17.2 (20–100 °C) 18.4 (20–538 °C)	193 (20 °C)	0.3	2–10
Ni[c]	8.9	1450 (1425–1450)	88 (20 °C) 62 (20–500 °C)	13.3 (20–100 °C) 16.3 (20–900 °C)	204 (20 °C)	0.3	3–7

[a] 3 mol % Y_2O_3-doped tetragonal zirconia polycrystal.
[b] Stainless steel 304.
[c] Nickel.

10 vol % (FGMs) and 100 vol % (DJMs) compositional gradient, and then compacted at the optimized pressure ($\leqslant 1$ ton mm^{-2}). TZP/(Ni, SUS304)-FGMs and DJMs were hot pressed at 1250 °C, 1 h in a nitrogen atmosphere and at 5 °C min^{-1} on heating and cooling to relax the residual stress. The hot pressing was used to control the sintering defects caused by the difference of sintering shrinkage between TZP and the metals.

The density of the sintered and surface-finished body was measured with the metal volume fraction by ASTM C2D. The measurement of hardness was carried out on the polished surface at room temperature with a Vicker's hardness tester (model DVKH-1, Japan). The compositional continuity via the distribution of metal elements was examined with an electron probe microanalyser (EPMA, JAX-8600, Jeol, Japan) and a wavelength dispersive spectrometer (WDS, JAX-8600, Jeol, Japan), and the microstructure and fractured surface morphology were observed by optical microscopy (Reichert Metaplan 2, Leica, Austria) and scanning electron microscopy (SEM, JSM-5200, Jeol, Japan). The CTEs of each composition were measured with a thermomechanical analyser (TMA, CN8098D2, Rigaku, Japan) in order to compare experimental values with calculated values applied for finite element analysis. The residual stress distribution of FGMs was analysed by the finite element method (FEM, Ansys-Version 4.4), compared with that of DJMs. In addition, the possibility of using FGMs as thermal barrier materials has been discussed in terms of thermal diffusivity and thermal conductivity by the laser flash technique with a thermal constant measuring instrument (TC-7000, Sinku-Riko, Inc., Japan), and compared with theoretically calculated values.

3. Results and discussion

3.1. Sintering characteristics and microstructure

The relative density and the porosity of each composition layer are shown in Fig. 3 as a function of metal volume fraction. At this time, the porosity was supposed to be the difference between theoretical and relative density. It can be expected that these pores will cause the relaxation of residual stress and increase the thermal properties from the viewpoint of thermal protection and thermal shock resistance [4]. However, control of porosity is required because of the degradation of mechanical properties. A relatively low density (88% R.D.) is obtained for ceramic (TZP)-monolith, resulting from the low sintering temperature which prevented the melting of metals. The rapid increase of relative density with the addition of the metal is thought to be induced by easy diffusion of the metal [24]. It was thought that the relatively low density in composites with > 90 vol % metal contents was due to the PVA binder added to form the green bodies and the pore trapped by the relatively rapid necking of the metal matix.

Fig. 4 shows the Vicker's hardness of each composition with the various metal volume fractions. The measured values are inversely proportional to metal

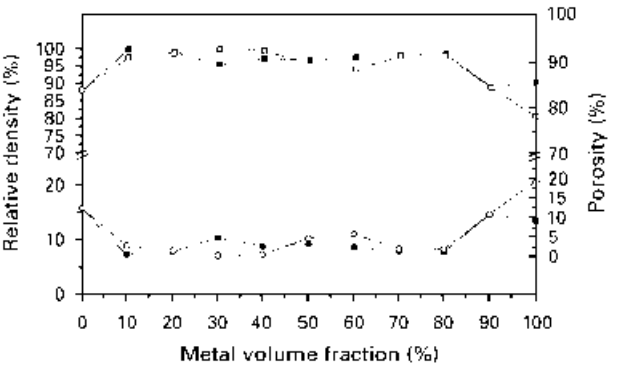

Figure 3 Effect of metal volume fraction on (■, □) relative density and (●, ○) porosity in the TZP-metal system: (■, ●) TZP-Ni composite, (□, ○) TZP-SUS304 composite.

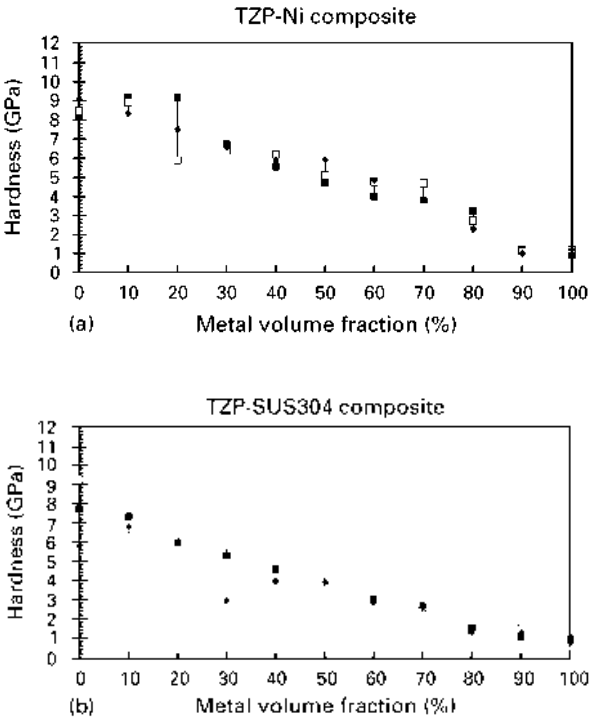

Figure 4 Effect of metal volume fraction on Vicker's hardness in the TZP-metal system: (a) TZP-Ni composite, (b) TZP-SUS304 composite. Average values of (◆) first, (■) second, and (□) third specimens.

volume fraction because the metal has relatively low hardness values. Generally, TZP/Ni composites appear to have higher hardness values than TZP/SUS304 composite because hardness is influenced by the sintering density and the intrinsic material properties [24]. So, the hardness of the composition layer with 10 vol % metal is not decreased by the effect of density.

The microstructure of FGMs and the distribution of metal elements (nickel and SUS304) are represented in Figs 5 and 6, respectively. It has been shown that despite stepwise stacking, the microstructure and the distribution of metal elements are gradually changed without distinct boundaries between the layers. The minimum thickness of one layer in FGMs by the P/M method is known to be about 0.2 mm with control of the composition being possible [4, 25]. However, FGMs with a layer thickness below 0.2 mm were obtained in this study, even though it is shown in

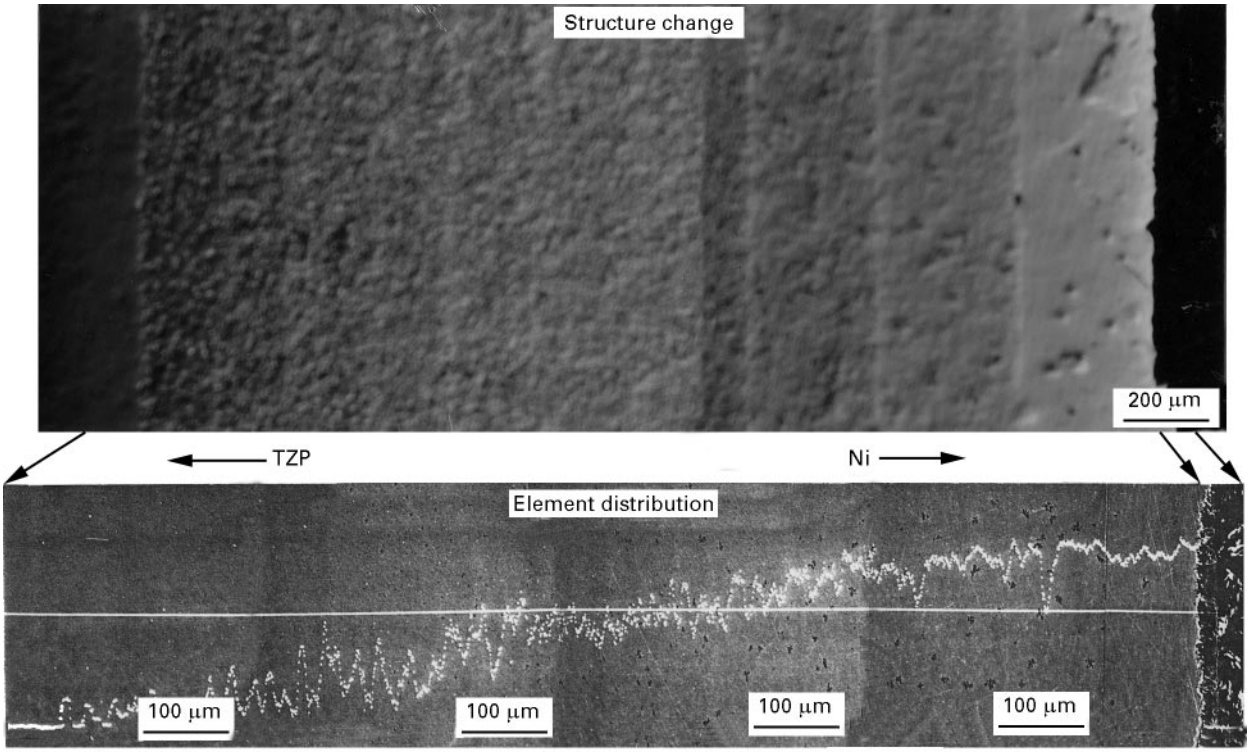

Figure 5 Multilayer structure and nickel distribution of the TZP/Ni-FGM with 10 vol % variation.

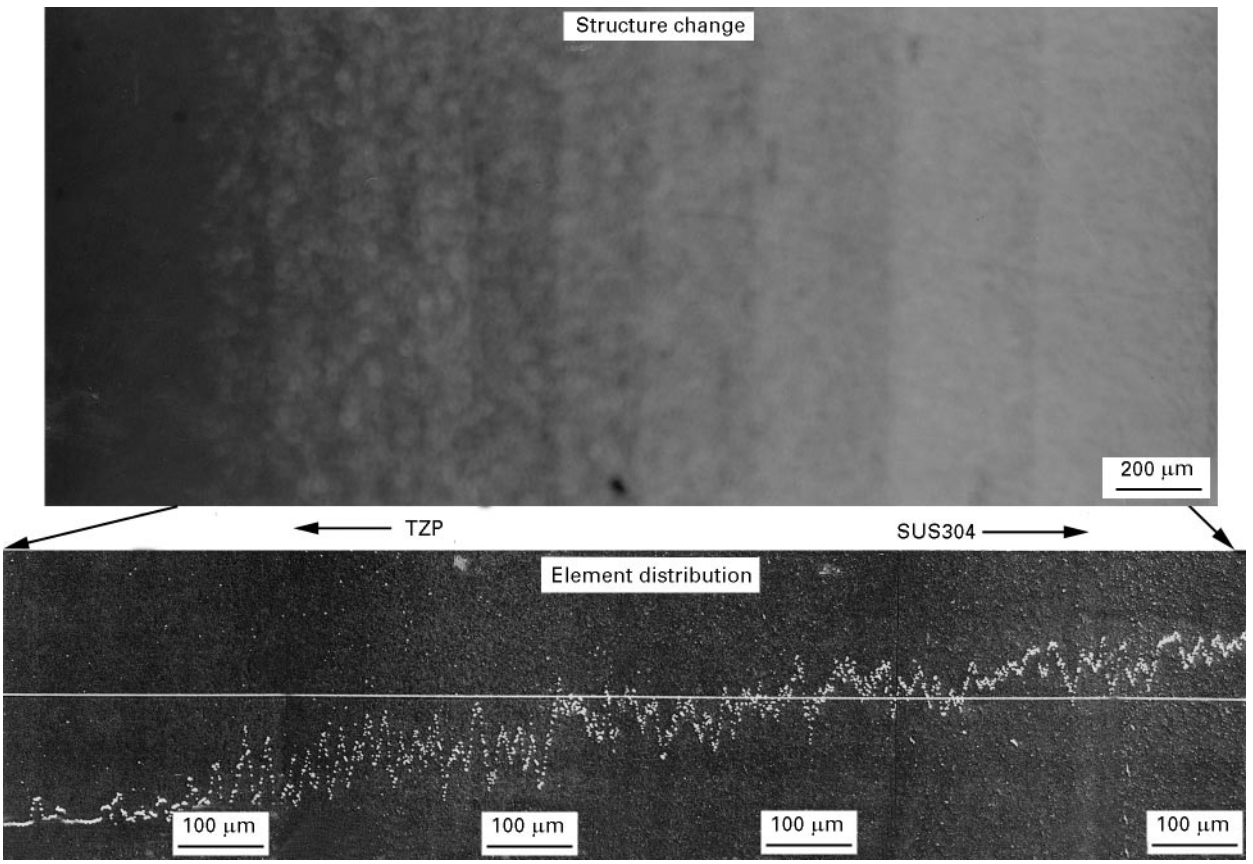

Figure 6 Multilayer structure and SUS304(Fe) distribution of the TZP/SUS304-FGM with 10 vol % variation.

TZP-rich regions. Because the layer thickness is dependent on the morphology of the particles and the fabrication process, if the particle size of starting materials and the layer thickness of the green body are optimized, the layer thickness after sintering will be controlled. The distribution of nickel and SUS304 observed with WDS are shown in Fig. 7 on a logarithm scale. Also, the compositional continuity of FGMs can be investigated.

The fracture surfaces of TZP/Ni- and TZP/SUS304-FGM are shown in Fig. 8. The crack formed vertical to the fracture surface, the debonding at the interface

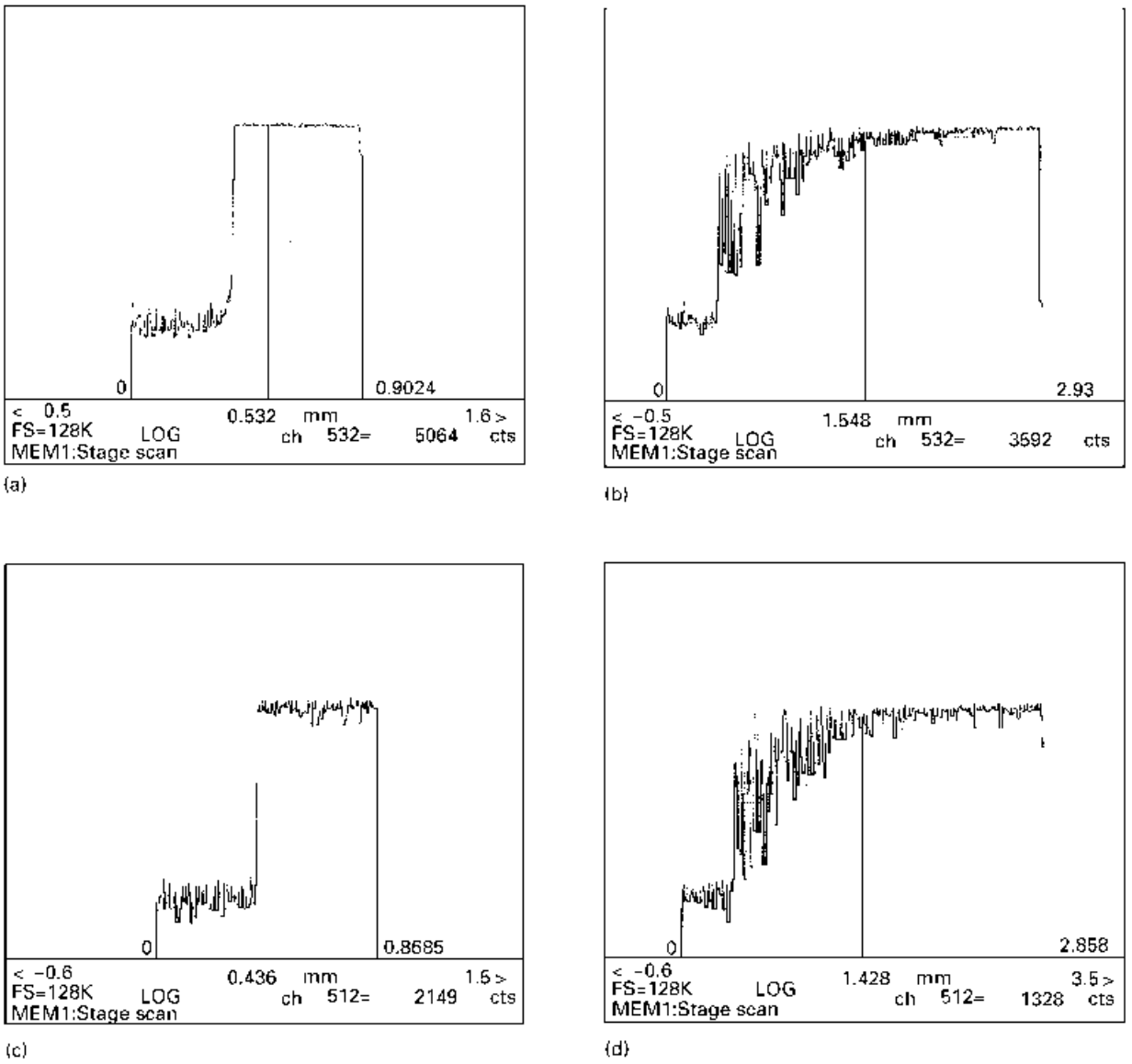

Figure 7 Element distribution as a function of the layer number by WDS: (a, b) nickel distribution, (c, d) SUS304(Fe) distribution. (a, c) Bonded material, (b, d) FGM.

around the metal, and the separated metal sites from fracture surface, were investigated through the fractographs of Fig. 8. It has been assumed that these phenomena are mainly due to residual stress. In particular, the fracture of metal (SUS304) is investigated in Fig. 8b because the residual stress generated at the interface is higher than that of the TZP/Ni system and the fracture strength of SUS304 is lower than that of nickel.

3.2. FEM analysis

The residual stress induced during the fabrication process plays a dominant role in the fracture of materials, which is unable to be applied under severe environments [2, 3, 8]. Therefore, for the relaxation of residual stress by optimized material design, the stress distributions formed at the interface and within the body of FGMs have been analysed by FEM [9–12, 26], and compared with that of DJMs. A common structure analysis program, Ansys (version 4.4A), was chosen for the finite element analysis. As the analysis model, a cylinder with axial symmetry was used, which is often utilized for standard sample of joining experiments and is relatively easy for the finite element analysis. As shown in Fig. 9, the mesh division was performed with a rectangular isoparametric element, and the numbers of node points and elements were 1403 and 1320, respectively. The two-dimensional model, only considering a change of two axes, was used as the boundary condition. Here, the analytical model was the same size as the fabricated specimen which was 30 mm diameter and 2.75 mm high. The thickness of each layer was assumed to be the 0.25 mm with uniformity, and that of the DJMs used for comparison was assumed to be the same as the FGMs. The material constants in each composition for finite element analysis, such as Young's modulus, CTEs and Poisson's ratio, were calculated from the equations below [27–29]

$$E_0 = E_c \frac{E_c + (E_m - E_c)V_m^{2/3}}{E_c + (E_m - E_c)(V_m^{2/3} - V_m)} \quad (1)$$

$$\alpha_0 = \frac{\alpha_m K_m V_m + \alpha_c K_c (1 - V_m)}{K_m V_m + K_c (1 - V_m)} \quad (2)$$

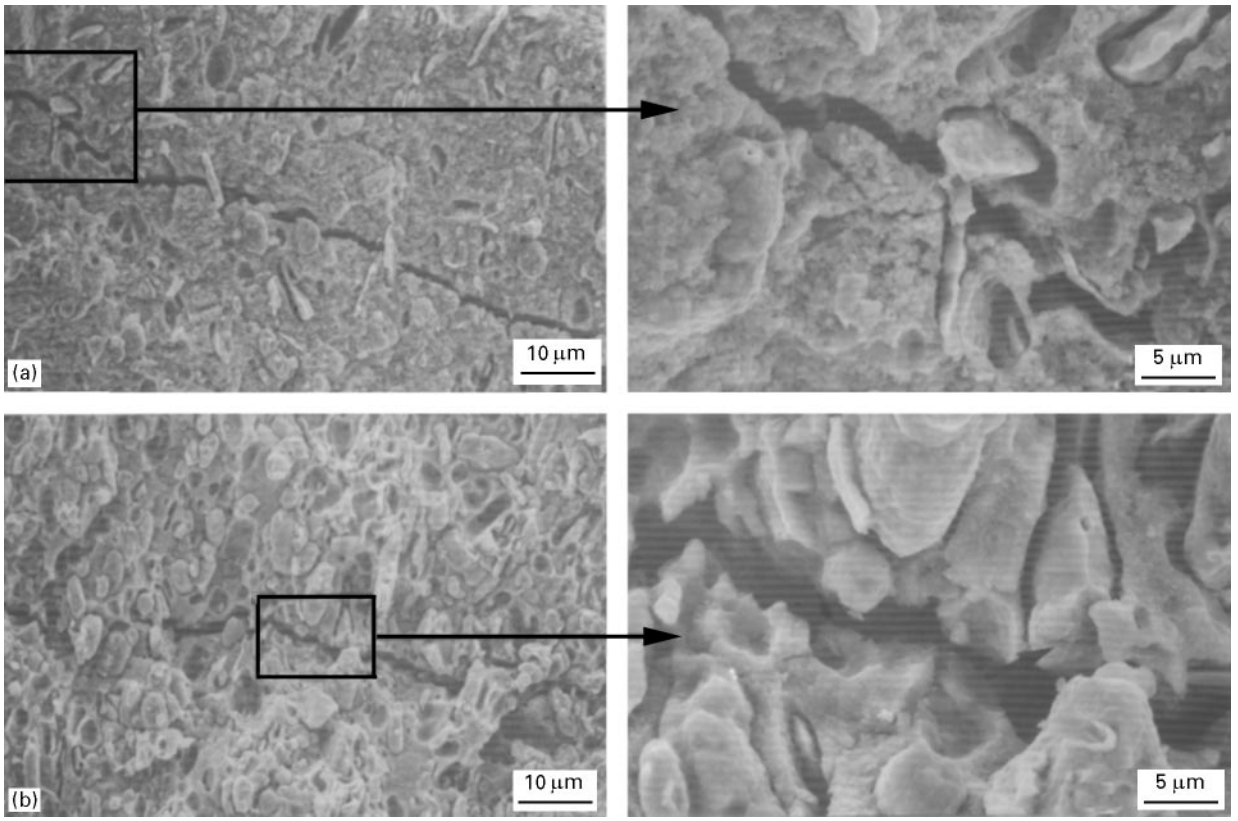

Figure 8 Scanning electron micrographs of the fracture surface in TZP/metal-FGMs with 10 vol % variation: (a) TZP/Ni-FGM and (b) TZP/SUS304-FGM.

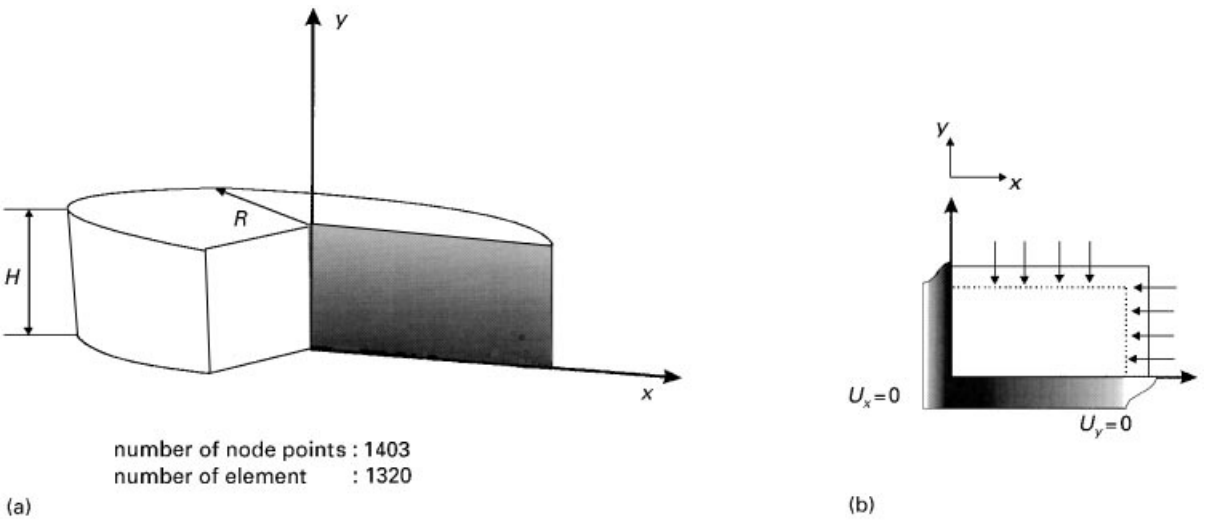

Figure 9 (a) Mesh division and (b) analytical model for finite element analysis.

$$\nu = \nu_c(1 - V_m) + \nu_m V_m \tag{3}$$

$$K_m = E_m/2(1 - \nu_m) \tag{4a}$$

$$K_c = E_c/2(1 - \nu_c) \tag{4b}$$

where subscripts c and m indicate ceramic and metal, and E_0, α_0 and ν_0 are Young's modulus, CTEs and Poisson's ratio of each composition, respectively. The effect of the change of Poisson's ratio on the residual stress in each composition is little, so Poisson's ratio can be expressed as a linear function of the position. Pores will be contained in the practical specimen, but we do not consider this effect in finite element analysis. As shown in Fig. 10, CTEs, the most important factor causing residual stress, were compared with experimental values. The experimental values approximately correspond to calculated ones, but the difference between the two CTEs (experimental and calculated) may be induced by the effects of pores not considered in above equations. So, no account is taken of the error caused by the application of calculated values.

In the case of the two-dimensional model, there are three stress components in the materials: σ_{xx} (radial stress), σ_{xy} (shear stress) and σ_{yy} (axial stress). Assuming that the analytical model was a perfect elastic

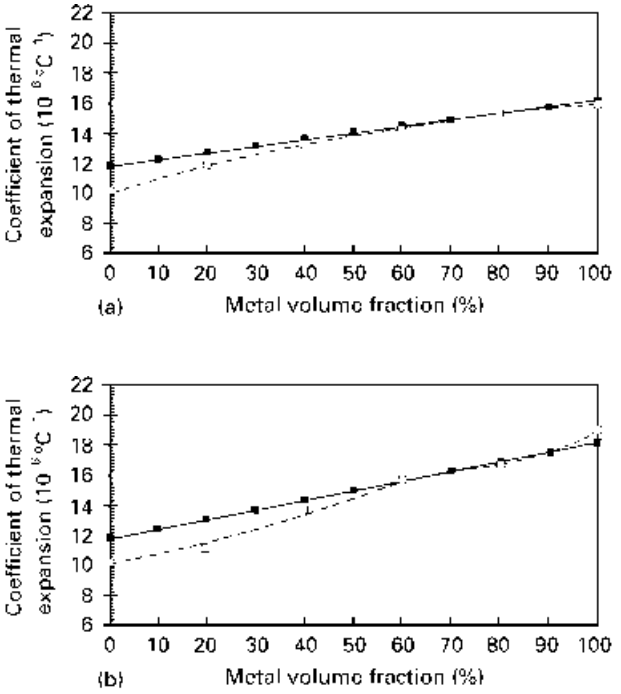

Figure 10 The average coefficient of thermal expansion of (a) TZP/Ni and (b) TZP/SUS304 composites from room temperature to 1000 °C. (□) Experimental CTEs, (■) calculated CTEs. The calculated CTEs of TZP/Ni and TZP/SUS304 composites are averaged over room temperature to 900 °C and 500 °C ranges, respectively.

body without plastic deformation, the distribution of residual stress induced during uniformly cooling from a fabrication temperature to room temperature ($\Delta T = 1230\,^{\circ}C$) is shown in Figs 11–14. In the case of DJMs (Figs 11 and 12), σ_{xy} and σ_{yy} components show a remarkable stress concentration at the edge, and tend to decrease quickly as the distance from the edge becomes greater. The σ_{xy} component shows the tensile stress in the edge regions. σ_{xx} exhibits the largest value at the centre of the top and bottom surfaces of the disc, and the stress concentration is built up in the vicinity of the interface. As a result, the severe stress concentration causing fracture of the material is induced at the interface and the edge. On the other hand, as shown in Figs 13 and 14, the residual stress produced during the fabrication process can be relaxed in the case of FGMs. The residual stress generated in TZP/Ni-FGM is relatively small in comparison with TZP/SUS304-FGM, because of smaller thermal expansion mismatch, from which we expect that FGMs with smaller thermal expansion mismatch will be stable during crack formation by residual stress.

From the results analysed so far, σ_{xy} generating tensile stress in most regions has been thought to be the main factor affecting crack formation. These opinions are in accordance with the analysis of Itoh and Kashiwaya [30], who reported in the case of a gradation plate that separation cracking may occur in the relatively small size gradation plate, $2R/H < 40$, and if $2R/H > 40$ then σ_{xx} and $\sigma_{yy} > \sigma_{xy}$ holds, and surface cracking may occur. Therefore, it can be verified by finite element analysis that the stress concentration in the materials is reduced by using the gradation technique; sound material will be obtained without the development of cracks under severe environments such as thermal barriers.

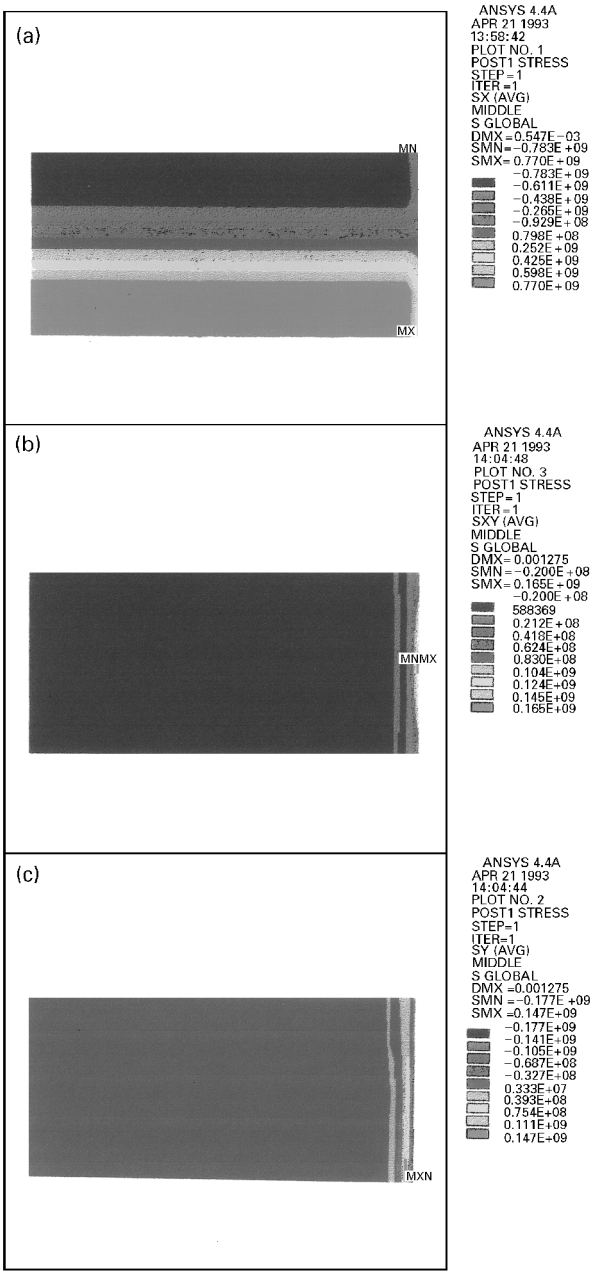

Figure 11 Residual stress distribution of directly jointed TZP/Ni: (a) σ_{xx} (radial stress), (b) σ_{xy} (shear stress) and (c) σ_{yy} (axial stress).

3.3. Thermal properties

In order to examine the thermal barrier properties, thermal conductivity was calculated from the following equations [27–29]

$$\lambda_0 = \lambda_c \left[1 + \frac{3(\lambda_m - \lambda_c)V_m}{3\lambda_c + (\lambda_m - \lambda_c)(1 - V_m)} \right] \tag{5}$$

$$\lambda = \frac{\lambda_0[(1-P)^{2/3}\lambda_0 + P^{2/3}\lambda_g]}{P^{1/3}\lambda_0 + (1-P)^{1/3}[(1-P)^{2/3}\lambda_0 + P^{2/3}\lambda_g]} \tag{6}$$

where λ_0 and λ are thermal conductivity with/without pores in materials, V is the volume fraction, and

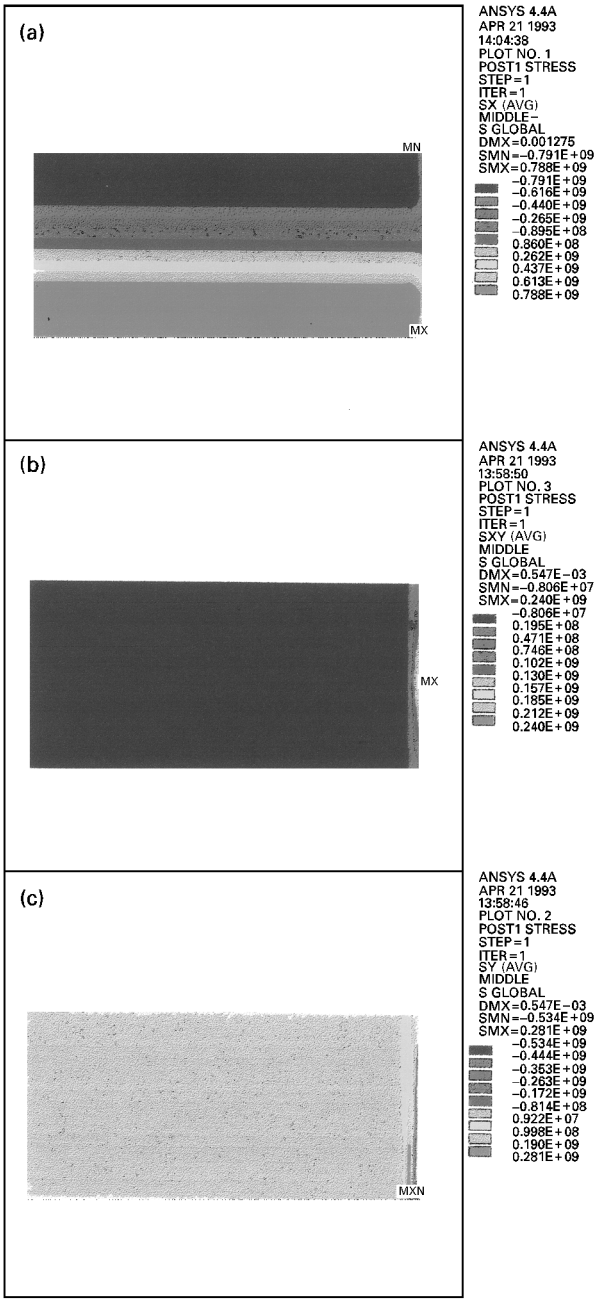

Figure 12 Residual stress distribution of directly jointed TZP/SUS304; (a) σ_{xx} (radial stress), (b) σ_{xy} (shear stress) and (c) σ_{yy} (axial stress).

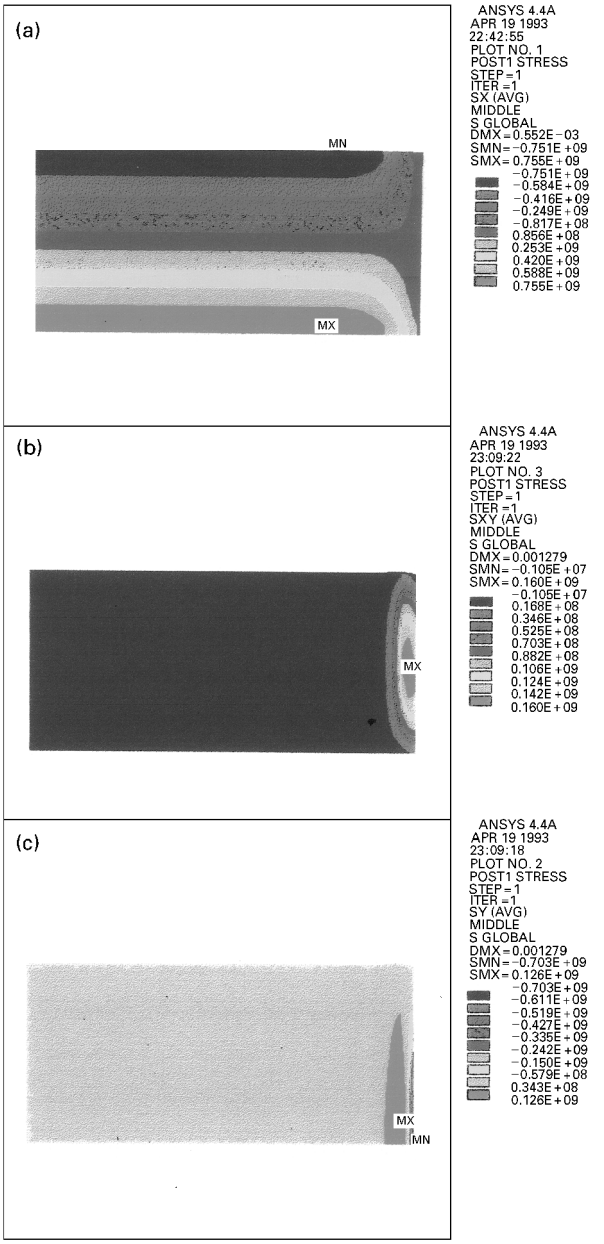

Figure 13 Residual stress distribution of compositionally gradient TZP/Ni: (a) σ_{xx} (radial stress), (b) σ_{xy} (shear stress) and (c) σ_{yy} (axial stress).

subscripts c, m and g are ceramic, metal and gas, respectively. The calculated thermal conductivity, as shown in Fig. 15, increases as the volume fraction of metal increases, resulting from higher thermal conductivity of the metal. In particular, the thermal conductivity of TZP/Ni composites noticeably increased. However, decrease of the thermal conductivity by the pores does not mean the degradation of the property, because the demand for thermal conductivity depends on the environments under which FGMs will be used.

To examine the thermal insulating properties of FGMs, the thermal diffusivity of FGMs and DJMs and the thermal conductivity of FGMs were measured by the laser flash technique [31–34]. From Fig. 16, showing the relationship between thermal diffusivity and temperature, it has been found that TZP/SUS304-FGM has the lowest value below 600 °C, and TZP/Ni-FGM appeared to have the lowest value from 600–800 °C. Above 800 °C, TZP/Ni-DJM had the lowest value. The changes of thermal diffusivity with temperature were mainly influenced by the intrinsic properties of nickel and SUS304. Because the interfacial stability and the relaxation of the residual stress must be considered, it cannot be confirmed that DJMs in terms of the thermal diffusivity only, are superior to FGMs as thermal barrier materials. The thermal conductivities of FGMs measured by the laser flash technique are shown in Table II. The thermal conductivity is inversely proportional to the thickness of the FGMs layer, and it is thought that the excellent thermal protection properties are due to the micropore and interface peculiarities. Finally, it has been recognized that the possibility of using FGMs as thermal barrier materials is greater than that of DJMs.

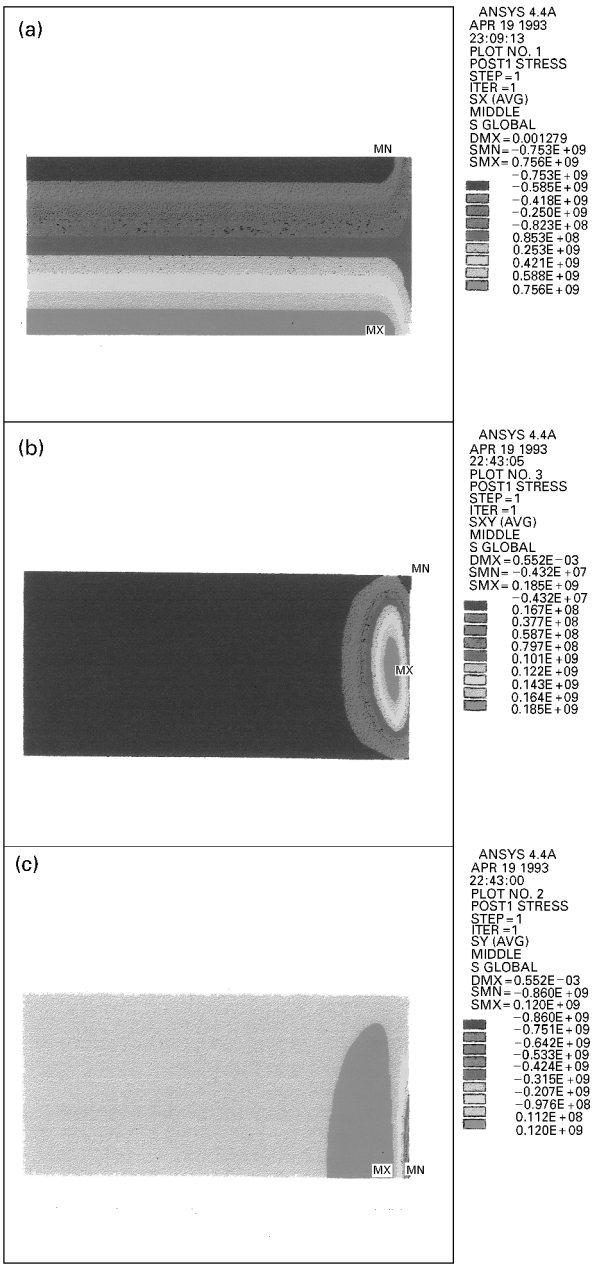

Figure 14 Residual stress distribution of compositionally gradient TZP/SUS304: (a) σ_{xx} (radial stress), (b) σ_{xy} (shear stress) and (c) σ_{yy} (axial stress).

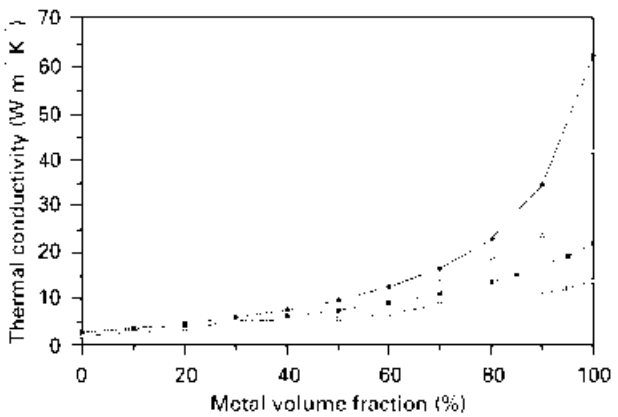

Figure 15 Effect of metal volume fraction and porosity on thermal conductivity in each (●, ○) TZP/Ni and (■, □) TZP/SUS304 composite. (●, ■) Theoretical values, (○, □) with pores.

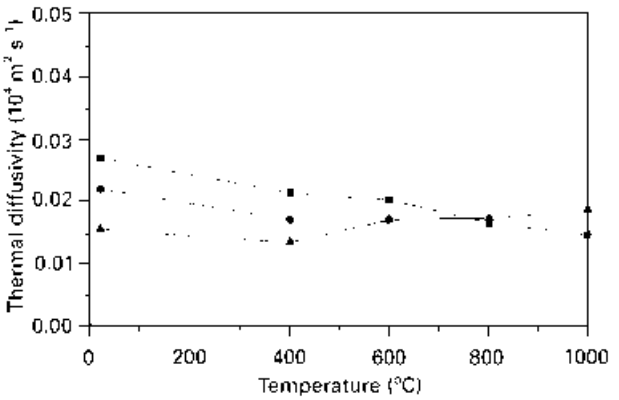

Figure 16 Effect of temperature and interlayer number on thermal diffusivity. TZP-Ni: (■) interlayer 0, (●) interlayer 9, (▲) TZP-SUS304, interlayer 9.

TABLE II Thermal conductivity measured by the laser flash technique

Materials	Case 1	Case 2
TZP	3.3	–
Ni	88	–
SUS304	16.2	–
TZP/Ni · FGM (10 layers)	6.55 (2.2 mm)	2.06 (3.9 mm)
TZP/SUS304 · FGM (10 layers)	7.13 (2.0 mm)	5.11 (3.0 mm)

4. Conclusion

TZP/Ni- and TZP/SUS304-FGM with 10 vol % compositional gradient were fabricated by hot pressing to improve the sintering defects. Here, the control of thickness was possible below 0.2 mm, and the compositional continuity of FGMs, though stepwise, was investigated by optical microscopy, EPMA and WDS. The material properties and the residual stress generated on cooling have an influence on the fracture of SUS304 particles in the TZP/SUS304 system.

There are two significant results from the finite element analysis of FGMs compared with DJMs. The first is the relaxation of the stress concentration and the residual stress induced on cooling from the sintering temperature. The residual stress generated in TZP/Ni-FGM is smaller than in TZP/SUS304-FGM; therefore, it has been verified that the difference in CTEs between two components is a major factor in the residual stress and crack formation. The other results is confirmation that shear stress, σ_{xy}, preferentially acts on the fracture of FGMs and DJMs in the case of a small size gradation plate, $2R/H < 40$. Therefore, it is expected that the fabrication of materials to be used in severe environments can be optimized through material design and selection having similar properties. The superior thermal protection properties of FGMs are confirmed by measuring thermal diffusivity and thermal conductivity. Consequently, considering all the properties, as above mentioned, it has been identified that TZP/Ni-FGM is excellent thermal barrier material and more stable than either TZP/SUS304-FGM or DJMs.

References

1. T. HIRAI, *J. Jpn Soc. Powder and Powder Met*. **37** (1990) 240.
2. WOLFGANG G. J. BUNK, in "Proceedings of the Ist International Symposium on FGM", Sendai, Oct-1990, edited by M. Yamanouchi, M. Koizumi, T. Hirai and I. Shiota (FGM Forum, Japan, 1990) pp. 1–2.
3. M. KOIZUMI, *ibid*., pp. 3, 4.
4. R. WATANABE and A. KAWASAKI, *J. Jpn Soc. Powder and Powder Met*. **39** (1992) 279.
5. M. NINO and Y. ISHIBASHI, *J. Jpn Soc. Compos. Mater*. **16**(1) (1990) 14.
6. O. KIMURA and T. KAWASHIMA, *J. Jpn Soc. Powder and Powder Met*. **34** (1987) 325.
7. O. KIMURA, *ibid*. **34** (1987) 518.
8. O. KIMURA and T. KAWASHIMA, *ibid*. **36** (1989) 1.
9. Y. ITOH, Y. ISHIWATA and H. KASHIWAYA, *Cent. Mem. Iss. Ceram. Soc. Jpn* **97** (1989) 747.
10. J. H. SELVERIAN, D. O'NEIL and S. KANG, *Am. Ceram. Soc. Bull*. **71** (1992) 1403.
11. J. H. SELVERIAN and S. KANG, *ibid*. **71** (1992) 1511.
12. M. L. SANTELLA, *Ceram. Bull*. **71** (1992) 947.
13. M. KOIZUMI, *Ceram. Eng. Sci. Proc*. **13** (1992) 333.
14. M. NINO, *Ceramics* **29** (1994) 179.
15. M. SASAKI and T. HIRAI, *Cent. Mem. Iss. Ceram. Soc. Jpn* **99** (1991) 1002.
16. Y. MIYAMOTO, *Ceramics* **29** (1994) 214.
17. M. NIINO and M. SASAKI, *J. IEE Jpn* **110** (1990) 35.
18. M. NIINO and T. KAWAI, *Electon. Mat*. **8** (1991) 103.
19. R. WATANABE, H. TAKAHASHI, M. TAMURA, I. SHIOTA, T. YOSHIDA and T. KURINO, "Functionally Gradient Materials" (FGM Forum, Japan, 1993) pp. 1–10.
20. O. M. AKSELSEN, *J. Mater. Sci*. **27** (1992) 1989.
21. Y. SHINOHARA, I. SHIOTA and R. WATANABE, *J. Jpn Soc. Compos. Mater*. **17** (1991) 179.
22. H. TAKEBE, T. TESHIMA, M. NAKASHIMA and K. MORINAGA, *J. Ceram. Soc. Jpn* **100** (1992) 387.
23. B. ILSCHNER, in "Proceedings of the Ist International Symposium on FGM" and (FGM Forum, Japan, 1990) pp. 101–6.
24. Y. G. JUNG and S. C. CHOI, *J. Kor. Ceram. Soc*. **31** (1994) 321.
25. A. KAWASAKI, H. HIROSE, H. HASHIMOTO and R. WATANABE, *J. Jpn Soc. Powder and Powder Met*. **37** (1990) 922.
26. A. KAWASAKI and R. WATANABE, *J. Jpn Inst. Metals* **51** (1987) 525.
27. W. D. KINGARY, H. H. BOWEN and D. R. UHLMAN, "Introduction to Ceramics" (Wiley, New York, 1976).
28. R. KONDO, "Porous Materials" (Gihoudo, Japan, 1986).
29. N. NODA and T. TSUJI, in "Proceedings of the Ist International Symposium on FGM" and (FGM Forum, Japan, 1990) pp. 339–44.
30. Y. ITOH and H. KASHIWAYA, *J. Ceram. Soc. Jpn* **100** (1992) 476.
31. Y. BAYAZITOGLU and M. N. OZISIK, "Elements of Heat Transfer" (McGraw-Hill, 1988).
32. J. P. HOLMAN, "Heat Transfer" (McGraw-Hill, 1981).
33. J. P. HOLMAN, "Experimental Method for Engineers" (McGraw-Hill, 1978).
34. Y. S. TOLUKIAN, "Thermal diffusivity", Thermophysical Properties of Matter, Vol. 10 (IFI/Plenum, 1980).

Received 15 September
and accepted 15 December 1995